Optical Detection of Interfering Pathways in Subfemtosecond Multielectron Dynamics

Aleksei M. Zheltikov,[1] Aleksandr A. Voronin,[1] Markus Kitzler,[2] Andrius Baltuška,[2] and Misha Ivanov[3]

[1]*Physics Department, M. V. Lomonosov Moscow State University, Vorobyevy gory, 119992 Moscow, Russia*
[2]*Institut für Photonik, Technische Universität Wien, Gusshausstrasse 27, A-1040 Wien, Austria*
[3]*NRC Canada, 100 Sussex Drive, Ottawa, Ontario K1A 0R6, Canada*

(Received 16 July 2008; published 14 July 2009)

We show how time-resolved coherent anti-Stokes Raman scattering can be used to identify interfering pathways in the relaxation dynamics of autoionizing transients in many-electron systems, on femto- and attosecond time scales. For coherent population of many states, autoionizing wave-packet dynamics is resolved. We identify bound-bound, continuum-bound, and bound-continuum-bound contributions and show that they leave distinct features in the total coherent anti-Stokes Raman scattering signal.

DOI: 10.1103/PhysRevLett.103.033901 PACS numbers: 42.65.Re

Rapidly developing attosecond technologies offer unique tools capable of resolving extremely fast electron dynamic processes [1]. Attosecond metrology strategies typically involve a measurement of the yield of charged particles or molecular fragments. This approach proved to be remarkably efficient for an attosecond spectroscopy of the relaxation dynamics of core-excited atomic systems [2], electron tunneling visualization [3], attosecond probing of molecular dynamics [4], direct measurement of few-cycle optical field waveforms [5], and time-resolving photoelectron emission from solid surfaces [6]. Analysis of charged-particle or molecular-fragment spectra, however, often faces difficulties related to an overlap of the contributions of multiple initial and/or final states, superimposing many ionization channels.

Selectivity of all-optical methods to a specific channel is successfully employed through the use of high-order harmonic generation (HHG) for time-resolved measurements. Recent examples include tracing proton motion in molecules [7], monitoring attosecond hole dynamics [8], and quantum-state-resolved measurements using high-order harmonic transient absorption spectroscopy [9]. Mukamel [10] has theoretically demonstrated that x-ray four-wave mixing can be employed to create and probe ultrafast electron dynamics in many-electron systems with attosecond resolution.

Here we show that coherent anti-Stokes Raman scattering (CARS) can provide femto- to attosecond temporal resolution while not only focusing on a specific process but also identifying and isolating, due to the high selectivity inherent in Raman techniques, interfering pathways contributing to this process. In contrast to HHG, CARS does not necessarily involve a strong perturbation of a quantum system by a high-intensity laser field, allowing attosecond time resolution to be achieved without a substantial modification of a system under study. For autoionizing (AI) electronic wave packets, the CARS signal involves both quasibound and continuum components of AI states. The corresponding pathways have well-defined relative phase shifts and/or different temporal dynamics. We show how these can be used to identify interfering pathways in the total signal and how the phase shift between the interfering transitions involving AI states can be retrieved by using CARS. Because of these interfering pathways, the AI dynamics cannot be characterized by a steady state absorption line but requires time-resolved spectroscopy.

Consider time-resolving autoionization of a multielectron wave packet with CARS. Pertinent work includes experimental [2] and theoretical [11–13] studies of time-resolving Auger decay and Fano-type autoionization using photoelectron spectroscopy and spectroscopic studies of AI states using CARS [14]. We consider an approach based on combining an attosecond extreme ultraviolet (xuv) pulse with a few-cycle laser pulse. The xuv pulse with carrier frequency ω_1, field amplitude $\mathcal{E}_1$, polarization vector $\mathbf{e}_1$, and envelope $f_1(t)$ plays the role of the pump. The laser pulse [carrier frequency ω_2, field amplitude $\mathcal{E}_2$, polarization $\mathbf{e}_2$, and envelope $f_2(t)$] plays the role of the Stokes. The pair excites coherent superposition of the Fano-type [12,15] AI resonances (inset 1 in Fig. 1). Time-delayed by τ a uv or xuv pulse [carrier ω_3, amplitude $\mathcal{E}_3$, polarization $\mathbf{e}_3$, and envelope $f_3(t-\tau)$] probes Raman-excited transients with detection at the anti-Stokes frequency $\omega_4 = \omega_1 - \omega_2 + \omega_3$. Similar to conventional four-wave-mixing schemes [16], generation of the anti-Stokes signal in the considered xuv-visible CARS arrangement can be regarded as scattering of the probe field off the grating induced by the xuv pump and laser Stokes fields.

We develop a description directly in the time domain, natural for dealing with time-resolved wave-packet dynamics. The wave function is $|\Psi\rangle = e^{-iE_g t}[a_0(t)|0\rangle + |\Delta\Psi\rangle]$, where E_g is the ground state energy and

$$|\Delta\Psi\rangle = |\Psi^{(1)}(t)\rangle e^{-i\omega_1 t} + |\Psi^{(2)}(t)\rangle e^{-i(\omega_1-\omega_2)t} + |\Psi^{(3)}(t,\tau)\rangle e^{-i(\omega_1-\omega_2+\omega_3)t}. \quad (1)$$

Here $|\Psi^{(1)}(t)\rangle = \sum_l a_l(t)|l\rangle$ describes intermediate excitation created by the pump. The Raman pair of pump and

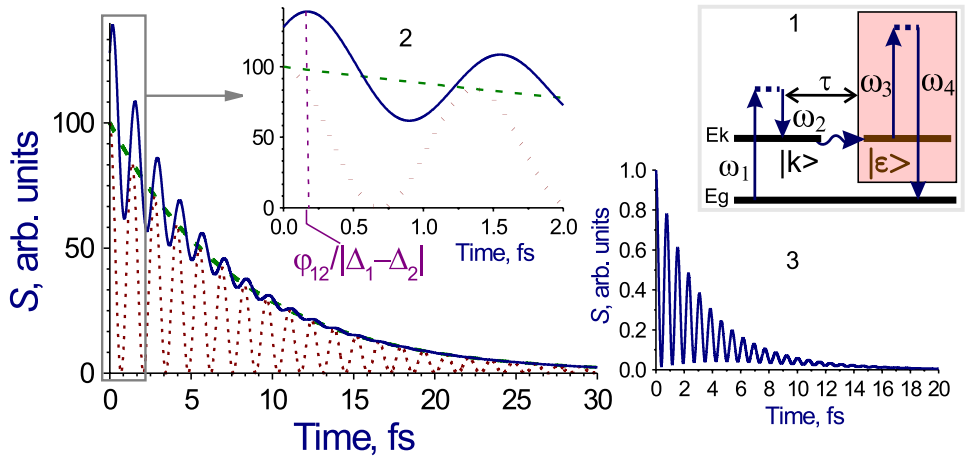

FIG. 1 (color online). Attosecond-resolved CARS signal for autoionizing wave packets. The dashed line shows the CARS signal for a single AI state with lifetime $1/(2\Gamma_1) = 8$ fs. The solid line shows the CARS signal from a superposition of two states spaced by $\Delta E = 3$ eV with $1/(2\Gamma_1) = 8$ fs, $q_{\text{pr-aSt},1} = q_{1,\text{pu-St}} = q_1 = 3$, $1/(2\Gamma_2) = 2$ fs, and $q_{\text{pr-aSt},2} = q_{2,\text{pu-St}} = q_2 = 1$. The dotted line shows the case of two states with equal CARS Fano parameters $q_1 = q_2 = 2$ and equal lifetimes $1/(2\Gamma) = 8$ fs. The pump and Stokes frequencies ω_1 and ω_2 are chosen such that $|\Delta_1| = |\Delta_2|$. The pump and probe pulse widths satisfy the inequalities $\Gamma_{1,2}T_{\text{pu,pr}} \ll 1$. A diagram of the CARS process is sketched in inset 1. Inset 2 shows a close-up view of the signal within the first two femtoseconds. Inset 3 displays time-resolved CARS signal from the $3s\,^1P^o$ and $4s\,^1P^o$ AI states in Ne.

Stokes pulses creates an AI wave packet $|\Psi^{(2)}(t)\rangle = \sum_k a_k(t)|k\rangle + \int d\epsilon c_\epsilon(t)|\epsilon\rangle$, where, following the standard approach [15,17], we use "bound" ($|k\rangle$) and "continuum" ($|\epsilon\rangle$) components of AI states coupled by the electron-electron correlation $\hat{W}$; ϵ denotes the detuning of the continuum state from the resonance energy $E_g + \omega_1 - \omega_2$.

Dynamics is monitored by the delayed probe pulse that creates $|\Psi^{(3)}(t,\tau)\rangle$ and induces the CARS polarization

$$\mathbf{P}(t,\tau) = a_0^*(t)\langle 0|\hat{\mathbf{d}}|\Psi^{(3)}(t,\tau)\rangle e^{-i(\omega_1-\omega_2+\omega_3)t}. \quad (2)$$

The standard procedure of perturbation theory then gives

$$\mathbf{P}(t,\tau) = \mathcal{E}_3 f_3(t-\tau)e^{-i(\omega_1-\omega_2+\omega_3)t}\Big[\sum_k \langle 0|\hat{\mathbf{D}}^{(2)}_{\text{pr-aSt}}|k\rangle a_k(t) + \mathbf{D}^{(2)}_{\text{pr-aSt},c}C(t)\Big], \quad (3)$$

where $\hat{\mathbf{D}}^{(2)}_{\text{pr-aSt}} = -\sum_j \frac{\hat{\mathbf{d}}|j\rangle\langle j|\hat{\mathbf{d}}\cdot\mathbf{e}_3}{E_j-[E_g+\omega_1-\omega_2+\omega_3]}$, $C(t) = \int d\epsilon c_\epsilon(t)$, and

$$c_\epsilon(t) = -i\int^t dt' e^{-i\epsilon(t-t')}\Big[\sum_k W_k a_k(t') + \mathcal{E}_1\mathcal{E}_2 f_1(t')f_2^*(t')D^{(2)}_{\text{pu-St}}\Big], \quad (4)$$

with $\hat{D}^{(2)}_{\text{pu-St}} = -\sum_l \frac{\mathbf{e}_2\cdot\hat{\mathbf{d}}|l\rangle\langle l|\hat{\mathbf{d}}\cdot\mathbf{e}_1}{E_l-[E_g+\omega_1]}$. Here we use the standard assumption in the Fano-type theory: The "bare" continuum $|\epsilon\rangle$ is assumed flat, with continuum structures appearing from the coupling between $|k\rangle$ and $|\epsilon\rangle$. Mathematically, this means $\langle\epsilon|\hat{D}^{(2)}_{\text{pu-St}}|0\rangle \approx D^{(2)}_{\text{pu-St}}$, $\langle\epsilon|\hat{W}|k\rangle \approx W_k$, and $\langle 0|\hat{\mathbf{D}}^{(2)}_{\text{pr-aSt}}|\epsilon\rangle \approx \mathbf{D}^{(2)}_{\text{pr-aSt},c}$.

The first term in square brackets in Eq. (4) describes a transition to the continuum via the quasibound part of the AI states $|k\rangle$. The second term describes direct excitation to the continuum. We assume that (i) there are no intermediate resonances at the probe step and (ii) the probe pulse is short compared to the decay time of the AI states: $\Gamma_k T_{\text{pr}} \ll 1$ for all $|k\rangle$. Here T_{pr} is the duration of the probe pulse, and Γ_k is the decay rate of the state $|k\rangle$.

Integrating over ϵ, we find

$$C(t) = -i\pi\Big[\sum_k W_k a_k(t) + \mathcal{E}_1\mathcal{E}_2 f_1(t)f_2^*(t)D^{(2)}_{\text{pu-St}}\Big]. \quad (5)$$

Now we can write CARS polarization Eq. (3) as

$$\mathbf{P}(t,\tau) = \mathcal{E}_3 e^{-i(\omega_1-\omega_2+\omega_3)t}[\mathbf{P}_{\text{ai}}(t,\tau) - i\mathbf{P}_c(t,\tau)], \quad (6)$$

where the direct contribution of the bare continuum is

$$\mathbf{P}_c(t,\tau) = \pi\mathbf{D}^{(2)}_{\text{pr-aSt},c}D^{(2)}_{\text{pu-St}}\mathcal{E}_1\mathcal{E}_2 f_1(t)f_2^*(t)f_3(t-\tau) \quad (7)$$

and the contribution of the AI wave packet is

$$\mathbf{P}_{\text{ai}}(t,\tau) = f_3(t-\tau)\sum_k a_k(t)(\mathbf{D}^{(2)}_{\text{pr-aSt},k} - i\pi\mathbf{D}^{(2)}_{\text{pr-aSt},c}W_k). \quad (8)$$

Three pathways interfere in the CARS signal. The first corresponds to the direct response of the flat continuum and is described by $\mathbf{P}_c(t,\tau)$ (the continuum-bound channel). It corresponds to the two-photon (pump-Stokes) Raman transition to the flat continuum followed by the two-photon (probe–anti-Stokes) transition back. The second and the third pathways both involve the AI state and enter via $\mathbf{P}_{\text{ai}}(t,\tau)$. The second pathway enters via $a_k(t)D^{(2)}_{\text{pr-aSt},k}$. It describes a response of the quasibound

component of the AI state (the bound-bound channel). The third, bound-continuum-bound channel, involves the quasibound component $|k\rangle$ as an intermediate step but probes the amplitude that has "leaked" into the continuum when the probe pulse arrives.

These pathways can be distinguished. Response of the flat continuum is instantaneous. As a result, no finite evolution time that would be related to electron wave-packet dynamics appears in $\mathbf{P}_c(t,\tau)$. Instead, this term follows the cross correlation of the Raman pump pair and the probe pulse; see Eq. (7). For pump and probe pulses much shorter than the AI lifetime, this cross correlation is followed by a much longer response associated with the AI wave packet, Eq. (8). The two components of this response are shifted in phase by $\pi/2$. We shall see that this phase shift can be used to identify the two pathways.

Equations (7) and (8) show that, for short pump and probe pulses ($\Gamma_k T_{\mathrm{pr,pu}} \ll 1$), the CARS signal directly traces dynamics of the AI wave packet. Indeed, at $\tau \gg T_{\mathrm{pu}}$ the pure continuum response $\mathbf{P}_c(t,\tau)$ is gone, and the CARS signal is dominated by $\mathbf{P}_{\mathrm{ai}}(t,\tau)$. With $\Gamma_k T_{\mathrm{pr}} \ll 1$, $a_k(t)$ in Eq. (8) can be replaced with $a_k(\tau)$. The integrated CARS signal is then given by $S(\tau) \propto \int dt |\mathbf{P}(t,\tau)|^2 \propto |\sum_k a_k(\tau)(q_{\mathrm{pr\text{-}aSt},k} - i)|^2$ and directly traces the wave-packet dynamics expressed by the interference of amplitudes a_k. The Fano parameter for the two-photon probe–anti-Stokes transition $q_{\mathrm{pr\text{-}aSt},k} = D^{(2)}_{\mathrm{pr\text{-}aSt},k}/[\pi D^{(2)}_{\mathrm{pr\text{-}aSt},c} W_k]$ controls the relative role of the two pathways in the CARS signal associated with the two components of the wave packet: the one still bound (contributing to the bound-bound pathway) and the one that has leaked into the continuum when the probe arrives (contributing to the bound-continuum-bound pathway.)

Standard perturbative calculation for $a_k(t)$ yields

$$a_k(t) = -i\mathcal{E}_1\mathcal{E}_2 F^{(2)}(\Delta_k,t) e^{-i(\Delta_k - i\Gamma_k)t}[\langle k|\hat{D}^{(2)}_{\mathrm{pu\text{-}St}}|0\rangle - i\pi W_k D^{(2)}_{\mathrm{pu\text{-}St}}]. \quad (9)$$

The first term in square brackets describes direct excitation to $|k\rangle$. The second describes excitation via continuum states coupled to $|k\rangle$ by electron-electron correlation $\hat{W}$. The transition amplitude is proportional to the Fourier component of the pump-Stokes two-photon envelope $f_1(t)f_2^*(t)$, with $F^{(2)}(\Delta_k,t) = \int_{-\infty}^{t} dt \times \exp(-i\Delta_k t) f_1(t) f_2^*(t)$, where $\Delta_k = E_k - (E_g + \omega_1 - \omega_2)$ is the detuning of the transition. With $\tau \gg T_{\mathrm{pu}}$, $F^{(2)}(\Delta_k,t) = \int_{-\infty}^{\infty} dt \exp(-i\Delta_k t) f_1(t) f_2^*(t) = F^{(2)}(\Delta_k)$.

Using Eq. (9) and introducing the Fano parameter for the pump-Stokes Raman transition $q_{\mathrm{pu\text{-}St},k} = D^{(2)}_{k,\mathrm{pu\text{-}St}}/[\pi D^{(2)}_{\mathrm{pu\text{-}St}} W_k]$, we obtain $S(\tau) \propto |\sum_k e^{-i(\Delta_k - i\Gamma_k)\tau}\alpha_k|^2$, and $\alpha_k = F^{(2)}(\Delta_k,t)(q_{k,\mathrm{pu\text{-}St} - i})(q_{\mathrm{pr\text{-}aSt},k} - i)$. The phase difference between the bound-bound and bound-continuum-bound pathways is $\phi_k = -\arctan(1/q_{\mathrm{pr\text{-}aSt},k}) - \arctan(1/q_{k,\mathrm{pu\text{-}St}})$.

When several states are populated, these phase shifts appear in the total signal. Figure 1 shows attosecond-resolved signals for one (dashed line) and two (solid and dotted lines) AI states. For one state (dashed line), we see a single-exponential decay. The CARS Fano parameters and the corresponding phase shift ϕ_1 have no impact on the time dependence of the CARS signal (here we selected $q_{\mathrm{pr\text{-}aSt},1} = q_{1,\mathrm{pu\text{-}St}} = 2$). Things change when the second state is present, with different CARS Fano parameters and therefore different phase shift ϕ_2. Here we set its lifetime at 2 fs and use smaller Fano parameters $q_{\mathrm{pr\text{-}aSt},2} = q_{2,\mathrm{pu\text{-}St}} = 1$. Spacing between the levels is set at 3 eV, which corresponds to an overlap of the electron energy spectra resulting from the AI decay. The center of the two-photon pump-Stokes transition is set in the middle between the levels, so that $|\Delta_1| = |\Delta_2|$.

Several features are visible in the plot. First, we see oscillations of the signal, characteristic of the wave packet. Second, oscillations decay with a time scale given by the lifetime of the shorter-lived state. Third, there is a phase shift in the oscillations as compared to the dotted line (see inset 2 in Fig. 1), where both states have equal Fano parameters $q_1 = q_2 = 2$ and hence equal ϕ_k. The phase shift between the two states $\phi_{12} = \phi_1 - \phi_2$ is mapped (see inset 2 in Fig. 1) onto the initial phase of the oscillating component of the CARS signal $2|\alpha_1||\alpha_2|\exp(-\Gamma_1 t - \Gamma_2 t)\cos[(E_1 - E_2)t - \phi_{12}]$.

The phase shift between AI wave packets can be retrieved through heterodyne CARS detection [18], which yields a signal $S_{\mathrm{het}}(\tau) \propto \mathbf{Im}[\int_{-\infty}^{\infty} dt \mathbf{E}^*_{\mathrm{lo}}(t,\tau)\cdot\mathbf{P}(t,\tau)]$ with a local-oscillator field at the anti-Stokes frequency

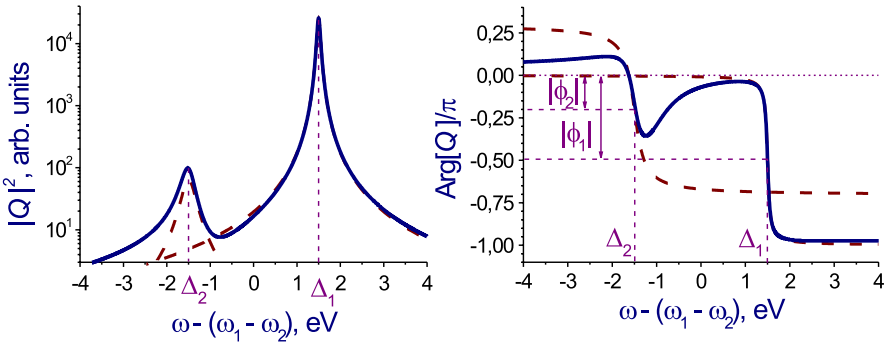

FIG. 2 (color online). The solid line shows the reconstruction of AI states from an attosecond-resolved heterodyne CARS signal for the parameters corresponding to the solid line in Fig. 1: (a) $|Q|^2 = |\int_{-\infty}^{\infty} dt \mathbf{P}_{\mathrm{ai}}(t,\omega)|^2$ and (b) Arg(Q). The dashed line presents (a) the spectra and (b) the phases for the two parts of Q related to the individual AI states contributing to CARS.

$\mathbf{E}_{\mathrm{lo}}(t,\tau) = \mathcal{E}_{\mathrm{lo}}\mathbf{e}_{\mathrm{lo}}f_{\mathrm{lo}}(t-\tau)e^{-i(\omega_1-\omega_2+\omega_3)t+\varphi_{\mathrm{lo}}}$, where $\mathcal{E}_{\mathrm{lo}}$, $\mathbf{e}_{\mathrm{lo}}$, $f_{\mathrm{lo}}(t-\tau)$, and φ_{lo} are the amplitude, polarization vector, temporal envelope, and adjustable phase shift, respectively, of the local-oscillator field. Setting φ_{lo} equal to $-\pi/2$ and 0, one can directly access the real and imaginary parts of the AI-related time-integrated nonlinear polarization $\mathbf{Q}(\tau) = \int_{-\infty}^{\infty} dt\mathbf{P}_{\mathrm{ai}}(t,\tau)$. In Fig. 2, we plot the modulus squared and the phase for the frequency-domain counterpart of $\mathbf{Q}(\tau)$, $\mathbf{Q}(\omega) = \int_{-\infty}^{\infty} dt\mathbf{P}_{\mathrm{ai}}(t,\omega)$, determined by taking the Fourier transform of the heterodyne CARS signal for AI states with different Fano parameters. This procedure, as can be seen from Fig. 2, correctly reconstructs the energies E_k, the lifetimes $1/(2\Gamma_k)$, and the phase shifts ϕ_k of AI states, resolving the spectra and the phases of individual AI states (shown by dashed lines in Fig. 2) in the measured CARS signal.

We now examine an application of the proposed CARS scheme to the $3s\,^1P^o$ and $4s\,^1P^o$ AI states in Ne. The relevant energies, lifetimes, and Fano parameters for these states are found from photoionization spectroscopy measurements [19], yielding $E_1 \approx 34.3$ eV, $E_2 \approx 39.6$ eV, $(2\Gamma_1)^{-1} \approx 8.2$ fs, $(2\Gamma_2)^{-1} \approx 20$ fs, $q_{1,\mathrm{pu\text{-}St}} \approx 40$, and $q_{2,\mathrm{pu\text{-}St}} \approx 45$. To probe these states using CARS, we apply linearly polarized Gaussian pump, Stokes, and probe pulses with $\hbar\omega_1 = 38.5$ eV, $\hbar\omega_2 = 1.5$ eV, $\hbar\omega_3 = 10$ eV, $T_{\mathrm{pu}} = 0.4$ fs, $T_{\mathrm{pr}} = 1$ fs, and $T_{\mathrm{St}} = 5$ fs, so that $\Gamma_{1,2}T_{\mathrm{pu,pr}} \ll 1$. The pump pulse is chosen short enough to provide efficient Raman excitation of AI states (the cross section of this process would be about 90 times lower with a 1-fs pump). The time-resolved CARS signal generated through the $\omega_4 = \omega_1 - \omega_2 + \omega_3$ wave mixing process displays oscillations (inset 3 in Fig. 1), originating from the interference of transitions involving the $3s\,^1P^o$ and $4s\,^1P^o$ AI states of Ne, with an oscillation period of 770 as. From the reference data [20], we estimate the absorption length for the anti-Stokes signal in neon at a pressure $p = 100$ mbar as 1 mm. The coherence (phase-mismatch) length at $p = 100$ mbar is $l_c = \pi(2|\mathbf{k}_{\mathrm{pu}} - \mathbf{k}_{\mathrm{St}} + \mathbf{k}_{\mathrm{pr}} - \mathbf{k}_{\mathrm{as}}|)^{-1} \approx 2$ mm, where $\mathbf{k}_{\mathrm{pu}}$, $\mathbf{k}_{\mathrm{St}}$, $\mathbf{k}_{\mathrm{pr}}$, and $\mathbf{k}_{\mathrm{aSt}}$ are the wave vectors of the pump, Stokes, probe, and anti-Stokes fields, respectively. In the regime of incoherent pump-probe spectroscopy of AI states, where the information about coherences is usually lost from the detected signal, phase matching is not required, and the parameter space for the experimental work is generally broader, but the spatial mode density of photons is lower.

In principle, the proposed spectroscopic technique can be implemented in an all-xuv format, i.e., without using the laser pulse. This can be done, e.g., through a $\omega_4 = \omega_1 + \omega_2 + \omega_3$ sum-frequency generation scheme, with all of the frequencies ω_1, ω_2, and ω_3 lying in the xuv range and corresponding to attosecond pulses. However, the role of a laser pulse becomes significant when a fine frequency tunability is needed for spectroscopy measurements, e.g., for the retrieval of the phase shifts of rapidly decaying eigenstates of a quantum system, such as AI states considered in this work. In the above discussion, we focused on a CARS process involving an AI state that can be coupled to the initial bound state by a two-photon-allowed Raman-type transition. Because of the odd parity of photons, one-photon transitions between these states are suppressed by parity conservation. Even when such one-photon transitions are allowed, CARS with an independent variable delay time introduced between the Stokes and pump pulses in addition to the delay time between the probe and Stokes pulses still offers an advantageous method for the analysis of ultrafast autoionization dynamics. Such a double-delay-time CARS, also referred to as two-dimensional CARS in molecular spectroscopy [21], can coherently project the interfering bound and continuum components of AI states excited by the pump photon to a bound-state wave packet, allowing a coherent control of population transfer via an AI state and helping to resolve dynamics related to the interfering quantum channels.

We acknowledge discussions with A. Stolow and O. Smirnova. We acknowledge support from the Max-Planck Institute for Quantum Optics (M. I. and A. Z.), A. von Humboldt foundation (M. I.), Russian Foundation for Basic Research (A. Z. and A. V.), and Austrian Science Fund (M. K. and A. B.).

[1] P. B. Corkum and F. Krausz, Nature Phys. **3**, 381 (2007).
[2] M. Drescher *et al.*, Nature (London) **419**, 803 (2002).
[3] M. Uiberacker *et al.*, Nature (London) **446**, 627 (2007).
[4] H. Niikura *et al.*, Nature (London) **421**, 826 (2003).
[5] E. Goulielmakis *et al.*, Science **305**, 1267 (2004).
[6] A. L. Cavalieri *et al.*, Nature (London) **449**, 1029 (2007).
[7] S. Baker *et al.*, Science **312**, 424 (2006).
[8] O. Smirnova *et al.*, Phys. Rev. Lett. **102**, 063601 (2009).
[9] Z. Loh *et al.*, Phys. Rev. Lett. **98**, 143601 (2007).
[10] S. Mukamel, Phys. Rev. B **72**, 235110 (2005).
[11] O. Smirnova *et al.*, Phys. Rev. Lett. **91**, 253001 (2003).
[12] M. Wickenhauser *et al.*, Phys. Rev. Lett. **94**, 023002 (2005).
[13] Z. X. Zhao and C. D. Lin, Phys. Rev. A **71**, 060702(R) (2005).
[14] A. M. Zheltikov *et al.*, JETP Lett. **54**, 139 (1991).
[15] U. Fano, Phys. Rev. **124**, 1866 (1961).
[16] G. L. Eesley, *Coherent Raman Spectroscopy* (Pergamon, Oxford, 1981).
[17] J. A. Armstrong and J. J. Wynne, in *Nonlinear Spectroscopy*, edited by N. Bloembergen (North-Holland, Amsterdam, 1977), p. 152.
[18] G. L. Eesley *et al.*, IEEE J. Quantum Electron. **14**, 45 (1978).
[19] C. McKenna *et al.*, J. Phys. B **37**, 457 (2004).
[20] B. L. Henke *et al.*, At. Data Nucl. Data Tables **54**, 181 (1993).
[21] G. Knopp *et al.*, J. Raman Spectrosc. **31**, 51 (2000).